The Analyses of Extended Shear Tab Steel Connections Part I: The Unstiffened Connections

ADEEB RAHMAN, MUSTAFA MAHAMID, AKEF AMRO, and AL GHORBANPOOR

Current practice uses steel plates and angles to frame beams into column flanges or webs. This practice requires coping of the beam flanges in the vicinity of the joint to bring the beam close to the web of the column. The extended shear tab connections are used to transfer the forces to the supporting member without the need for coping. Many cases of these connections were tested in the laboratory to help find their failure limit states and to develop design procedures for extended shear tab connections that could lead to significant savings in time and cost during construction (Sherman and Ghorbanpoor, 2002). This paper presents a 3D finite element (FE) model to validate the experimental results. This model will be expanded to analyze a number of different connection configurations such as deep connections with different bolt configurations. Other loading configurations can also be analyzed.

The failure mechanisms of steel connections must be considered in the design stage. The finite element method is well suited to study this problem because it is capable of solving complex geometries and nonlinearities in structural analysis problems. The predicted failure modes are compared to the experimental findings and to the limit states provided by the American Institute of Steel Construction (AISC) *Manual of Steel Construction* (AISC, 1994), hereafter referred to as the AISC Manual. The results from the experimental and the computational investigations introduce new limit states that should be considered in the design of extended shear tab connections.

Adeeb Rahman is associate professor, department of civil engineering and mechanics, college of engineering and applied science, University of Wisconsin–Milwaukee, Milwaukee, WI.

Mustafa Mahamid is structural engineer, Graef, Anhalt, Schloemer, and Associates, Milwaukee, WI.

Akef Amro is structural engineer, Atkins Highways & Transportation, Almondsbury, Bristol, UK.

Al Ghorbanpoor is professor, department of civil engineering and mechanics, college of engineering and applied science, University of Wisconsin–Milwaukee, Milwaukee, WI.

EXPERIMENTAL WORK

The experimental work considered here consisted of structural frames with three-bolt, unstiffened shear tabs and five-bolt, unstiffened shear tabs as shown in Figures 1 and 2 (Sherman and Ghorbanpoor, 2002). The dimensions for the components in the experiments are presented in Tables 1 and 2.

Linear velocity displacement transducers (LVDTs) were placed on the top flange of the beam to measure deflections and they are located at 1 in. from the corner of the top flange. Three pairs of strain gauges numbered 101/102, 103/104, and 105/106 were mounted on the top and bottom flange of the beam to calculate the load eccentricity using Equation 1 in the connection as shown in Figures 1 and 2. Strain gauges numbered 107, 108, 109, 110 and a rosette strain gauge were placed on the shear tab to study its stress and twist behavior (gauges 108 and 110 are mounted on the back side of the shear tab); these strain gauges are shown in Figure 3. The rosette strain gauge was placed on the shear tab to monitor the principal strains. The rosette consisted of three strain gauges labeled 201, 202, and 203 in the models presented as shown in Figure 3. Three readings were recorded in the strain gauges during the experiment. The principal strains are obtained using Equation 2 (Dally, 1978); where in the finite element model the principal strains are read directly at the location of the gauge (first principal strain). Finally, load cells were used to measure the applied load on the beam and the beam end reaction. A linear regression analysis was used to obtain the location of zero strain at each shear value. Equation 1 is used to determine the eccentricity, e, using the strain gauge readings.

$$e = \frac{\sum_{i}^{n} x_i \sum_{i}^{n} x_i y_i - \sum_{i}^{n} y_i \sum_{i}^{n} x_i^2}{N \sum_{i}^{n} x_i y_i - \sum_{i}^{n} x_i \sum_{i}^{n} y_i} \tag{1}$$

Table 1. Member Dimensions for the Three-Bolt Connection				
Member	**Category**	**Length**	**Thickness**	
Beam	W12×87	30 ft (9144 mm)	n.a.	
Column	W8×31	8 ft (2438.4 mm)	n.a.	
Shear tab	Extended	8.36 in. (212.34 mm)	0.375 in. (9.525 mm)	
Bolt	A325-X	n.a.	Shank Diameter	0.75 in. (19.05 mm)

Table 2. Member Dimensions for the Five-Bolt Connection				
Member	**Category**	**Length**	**Thickness**	
Beam	W18×71	20 ft (6096 mm)	n.a.	
Column	W14×90	8 ft (2438.4 mm)	n.a.	
Shear tab	Extended	11.54 in. (293.12 mm)	0.50 in. (12.7 mm)	
Bolt	A325-X	n.a.	Shank Diameter	0.750 in. (19.05 mm)

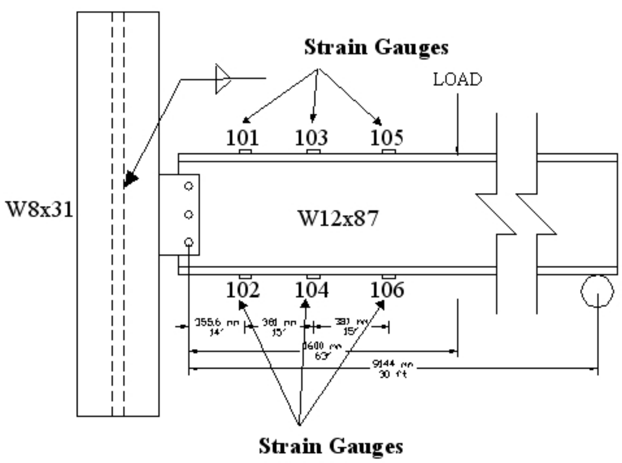

Fig. 1. Structure setup for three-bolt connection.

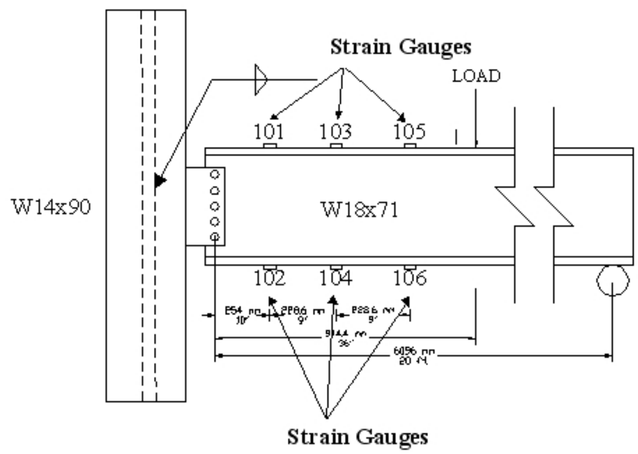

Fig. 2. Structure setup for five-bolt connection.

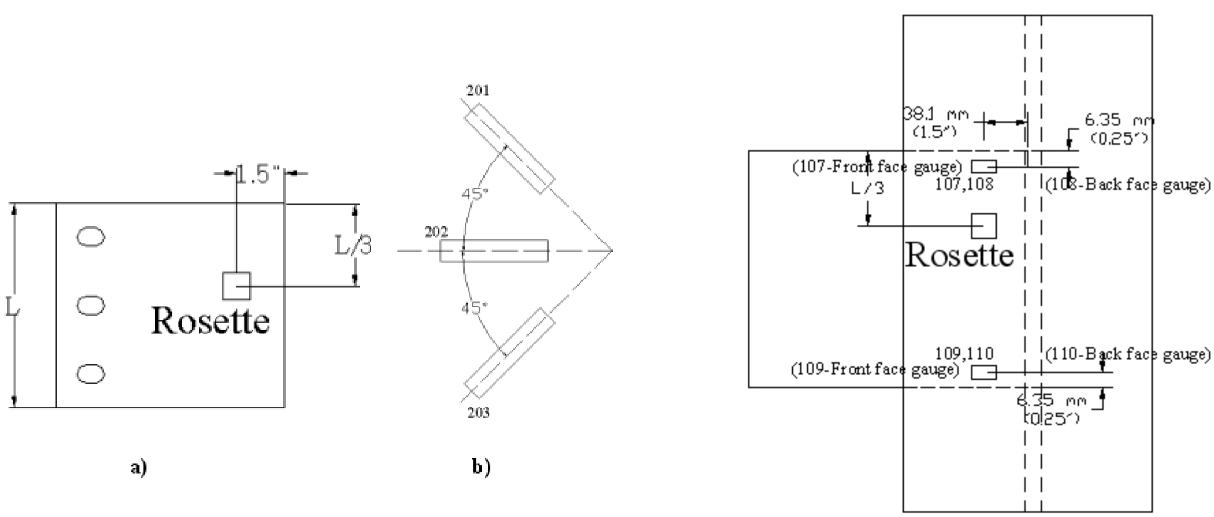

Fig. 3. Plate strain gauges (gray gauges are in the back) and rosette type and location used in the experiment.

Table 3. Contact Information for the Three-Bolt and Five-Bolt Connections						
Location	Stiffness Value	Friction Between Surfaces	Penetration	Contact Area	Target Area	Notes
Beam web and shear tab	0.3	0.3	Excluded	Shear tab	Beam web	One contact pair
Shear tab and bolt heads	0.3	0.3	Excluded	Bolt head	Shear tab	Separate contact pair for each bolt
Beam web and bolt heads	0.3	0.3	Excluded	Bolt head	Beam web	Separate contact pair for each bolt
Bolt pins and beam and shear tab holes	0.15	0.3	Excluded	Bolt pin	Beam and shear tab holes	Separate contact pair for each bolt

where

x_i = distance between the bolt line and each strain gauge pair (in.)

y_i = absolute value of the average strain gauge readings for each pair (in./in.)

n = number of strain gauge pairs

N = total number of strain gauges

$$\varepsilon_{principal} = \frac{\varepsilon_{201} + \varepsilon_{203}}{2} \pm \frac{1}{\sqrt{2}}\sqrt{\left(\varepsilon_{201} - \varepsilon_{202}\right)^2 - \left(\varepsilon_{202} - \varepsilon_{203}\right)^2} \tag{2}$$

where

$\varepsilon_{principal}$ = principal strain in rosette

ε_{201}, ε_{202} and ε_{203} = strain gauge readings

3D FINITE ELEMENT MODELING—NONLINEAR ANALYSIS

Measured geometrical dimensions of components were used to construct the finite element models in this study. This allows accurate comparison of the finite element analysis (FEA) results with the experimental results. The finite element program ANSYS was used to perform the required analysis. Four element types are used in the modeling of beams, columns, shear tabs, bolts, and contact surfaces. These elements are:

1. 3D, eight node, brick elements to model the beam, supporting members, and the shear tab. This element has elastic and plastic behavior capabilities and is suitable for modeling steel components.

2. 3D, 10-node, tetrahedral elements to model the bolts. The element has curved edges suitable for the bolt geometry. This element also has elastic and plastic capabilities and is suitable for modeling steel components.

3. Pretensioning elements to model the pretensioning force in the bolts. For the modeling of the bolt pretension, the bolt is modeled as one volume and is divided into two parts, separated by a pretension section that consists of pretensioning elements. A pretension force must be applied on this section to generate the required force in the bolt.

4. Contact elements to create contact surfaces to transfer the forces from the beam to the shear tab and to the bolts.

Friction, which is one of the most important parameters in defining contact surfaces, plays a main role in transferring forces between surfaces. The contact surfaces include: interfaces between the beam web and the shear tab, the beam and the bolt head, and the shear tab and the washer. There are also contact surfaces between the bolt shank and both the bearing surfaces of the holes in the shear tab and the beam web. Contact locations are shown in Table 3. Surface-to-surface and flexible-to-flexible contact type is used in the models to represent deformable steel contact surfaces in the connections. For each contact pair there is a contact and target area. The contact area is generally the smaller area with finer mesh, where the target area is the larger area with coarser mesh. Contact and target areas for each contact pair are shown in Table 3. Special attention is given to element divisions and mesh refinement.

The modeling starts with a transition from coarse mesh to finer meshes until the results cease to change. In addition, the lines in the model are divided to create elements and nodes at the locations of the LVDTs in the beam and strain gauges in the shear tab and in the beam in the actual experiments to allow accurate comparing of the FEA results with the experimental results. The contact elements, which overlay the solid elements, take the division of the underlying solid elements in the shear tab, beam web, and bolts. Element statistics for the element type are shown in Table 4. Figure 4 shows the 3D finite element model for the three-bolt connection and

Table 4. Elements Information for the Three-Bolt and Five-Bolt Connections			
Type of Element	**Location**	**Number of Elements**	
		Three-Bolt Connection	**Five-Bolt Connection**
SOLID185 (ANSYS)	Beam, column and shear tab	6,081	9,221
SOLID187 (ANSYS)	Bolts	756	1,288
CONTA174 (ANSYS) & TARGE170 (ANSYS)	Between beam web and the shear tab	2,237	3,603
	Between shear tab and bolt heads	2,997	11,770
	Between beam web and the bolt head and nut	3,798	6,385
	Between bolt shank and beam and shear tab holes	240	490
PRETE179 (ANSYS)	Bolt shank	116	154
Total		16,225	32,911

Figure 5 shows the shear tab and the supporting column for the five-bolt connection.

After generating the geometry and the mesh, three load steps are applied:

1. Applying the pretensioning force in the bolts. The pretensioning force value for the fully tight connections is 30 kips and for the snug-tight connections is 18 kips. The three-bolt and the five-bolt connections discussed in this paper are fully tight and 30 kips pretensioning force is used in the model. Several pretensioning force values were used starting from 5 kips and ending with 30 kips. The purpose of using small pretensioning values is first, to establish the contact surfaces between the shear tab

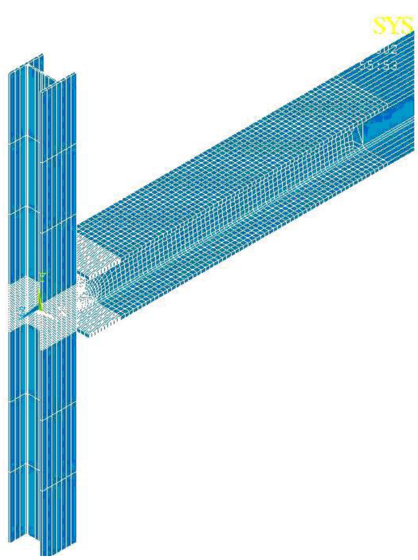

Fig. 4. 3D finite element model for the three-bolt connection.

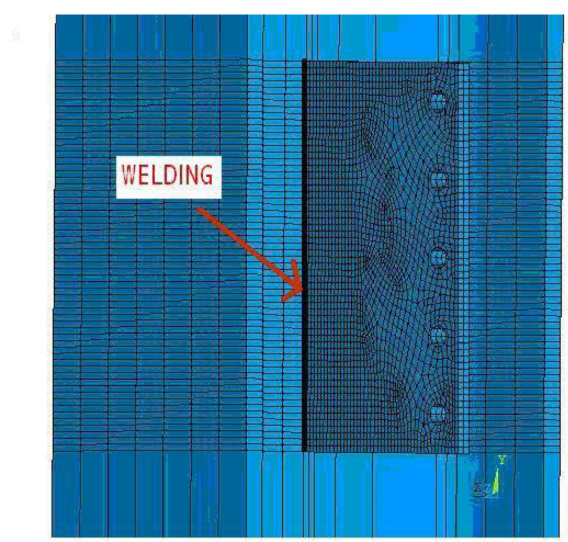

Fig. 5. Shear tab and supporting column for the five-bolt connection.

and the beam web, and between the bolt shank and the holes of the shear tab and the beam web, and second, to obtain the optimum pretensioning force that correlates the finite element results with the experimental results. The number of substeps required for this load step to obtain convergence is 2000. The pretensioning force value is in agreement with the pretensioning force recommended by AISC.

2. The second load step is also related to the pretensioning force, and it is part of the pretensioning process (ANSYS, 2001). It consists of one substep that converts the stresses due to the applied pretensioning force into strain. This load step is considered as locking the bolts and makes the structure ready to take external loads.

3. The third load step is the service load applied on the beam. The number of substeps for this load step varies depending on the applied load. The number of substeps for the three-bolt connection ranges from 500 to 2000 substeps. The number of substeps for the five-bolt connection ranges from 500 to 5000 substeps. Due to the existence of the contact elements, which cause high nonlinearity, and due to the plasticity in the steel materials, the model needed a large number of iterations to achieve accuracy and convergence. The run time also increases with the number of substeps. A typical run-time on a Pentium III PC is 5 hours for the three-bolt connection and 7 hours for the five-bolt connection to reach the failure load.

RELEVANT PARAMETERS FOR THE FE MODEL

Initially, convergence was difficult to achieve due to several parameters such as pretensioning force, coefficient of contact stiffness, and coefficient of friction. The coefficient of contact stiffness is a critical parameter in establishing contact between surfaces and in obtaining convergence. The recommended range for the contact stiffness coefficient for the type of contact mentioned above is 0.001 to 0.1. Penetration between the surfaces in contact occurs when using the low contact stiffness coefficient and convergence becomes more difficult as the coefficient of contact stiffness increases. The analysis began with a value of 0.001 to obtain convergence and was increased gradually until there was no penetration and convergence was achieved using a coefficient of contact stiffness of 0.03. These iterations were done during the first load step.

During the third load step, contact stiffness needs to be updated when the stresses in the structural components and in the bolts exceed the yield capacity. In this stage, the steel material looses stiffness and convergence becomes difficult. Since the stiffness of the contact elements is a function of the stiffness of the underlying materials, it needs to be updated accordingly. This could be done either manually or automatically in the finite element code. In this case, an option was activated to automatically update the contact stiffness with every sub-step to improve convergence and accuracy.

Coefficient of friction is another parameter that affects convergence as mentioned earlier; however, in this case it had a greater affect on the results. Coefficient of friction between the steel surfaces is provided by the AISC Manual (AISC, 1994) in the range of 0.2 to 0.6. A high coefficient of friction value causes convergence problems during the first and the third load steps and results also in a stiffer structure. Several values of the coefficient of friction in the range mentioned earlier were used in the model to achieve convergence up to failure. As a result, an optimum coefficient of friction of 0.3 was obtained and produced convergence through failure with accurate results as compared to the experimental outcome. The following solution options were used to achieve convergence: several values of contact stiffness were used, starting from a low value, until establishing the contact with convergence; loading substeps (maximum 200,000 and minimum 10) were used for pre-tensioning the bolts and establishing the contact; and a sparse solver was used because it is appropriate for this type of material and analysis (ANSYS, 2001). Penetration was excluded in all parts of the contact. A line search option was turned on for a nonlinear solution to improve and accelerate the convergence (ANSYS, 2001). The maximum number of iterations equaled 500 for each substep and the convergence criterion was set from 0.001 to 0.01, both of which are suitable for structural applications. With a 0.001 convergence criterion, convergence becomes difficult and it is used for applications where high accuracy is required, such as with biomedical and nuclear applications, whereas, a 0.01 convergence criterion is adequate for structural applications. This adjustment is to improve the convergence criteria. The contact stiffness for each contact pair is tabulated in Table 3.

Material Properties

The shear tab material in this study is ASTM A36, the bolt material is ASTM A325 (threads excluded), and the structural members are ASTM A572 Gr. 50 steel. A coefficient of friction equal to 0.30 is used. The stress-strain curve is used as input for the shear tab, bolts, and the column web. The curves were generated experimentally for each material. In the FE model with the three-bolt and five-bolt connections, the experimental stress-strain responses are specified in Figure 6. The stress-strain response for the bolts is shown in Figure 7.

Boundary Conditions and Loading

In the experiment, the column ends are secured against a vertical reaction wall. In the FE model, the nodes at the same location, which is 1 ft from the top and the bottom, were restrained in three directions. The beam ends are supported on rollers away from the connection. The boundary conditions are prescribed as such to represent in the model the experimental setup. Because the welding in the experiment was not a critical failure mode, in other words, connections did not fail in the welds in the actual experiments, the weld lines between the shear tab and the column web are modeled as continuous. The shear tab and the column web were modeled to have the same number of divisions in the vicinity of the shear tab as shown in Figure 5. After generating the mesh, these nodes are merged to obtain continuity at this location. A view of the finite element model in the connection vicinity is shown in Figure 8.

RESULTS AND DISCUSSION

Several parameters were established in studying the behavior of the unstiffened extended shear tab connections in the experimental and the FEA studies to estimate the load car-

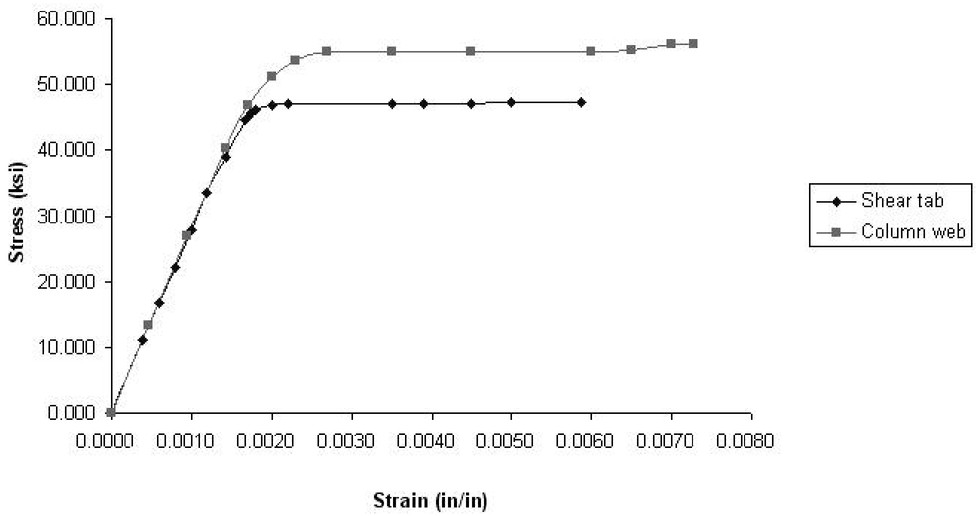

Fig. 6. Stress-strain curve for shear tab and column web.

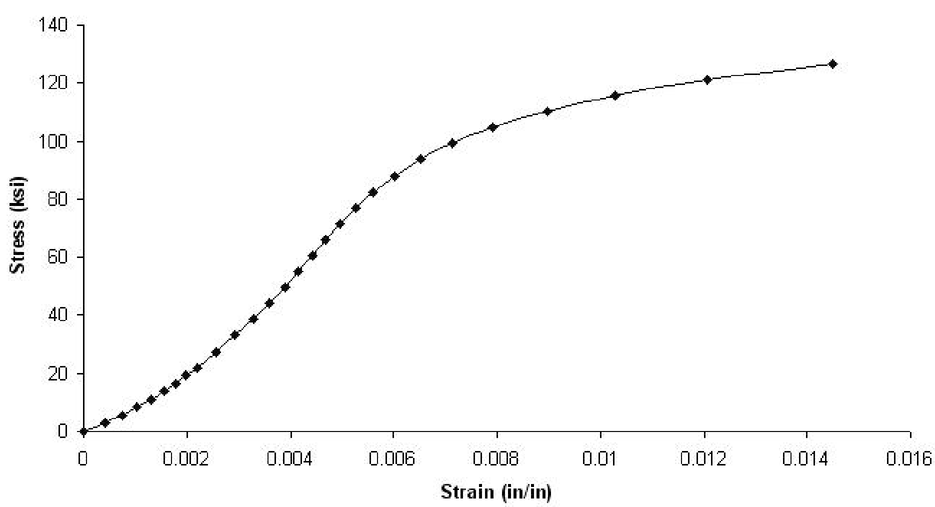

Fig. 7. Stress-strain curve for ASTM A325 bolts.

rying capacity as a function of the applied shear force at the connection. These parameters are: vertical displacement of the connection along the bolt line, shear load eccentricity relative to the connection bolt line, twisting of the connection plates, nonlinearity, and failure modes.

Vertical Displacement

In this study, finite element models were developed for three- and five-bolt connections to establish the governing analytical parameters to achieve good accuracy in the results. In the FEA, shear-displacement curves are considered to determine the ultimate capacity of the connection. The shear-twist curves are not considered in the FEA due to the fact that in the experiments, the only connection that failed primarily in twist failure mode was the five-bolt connection. The shear-displacement curves indicate the point at which the connection behavior becomes nonlinear; beyond this point the connection is still able to resist higher loads, but the respective curve begins to level off. The yield point does not represent imminent failure, but several conditions, such as: shear distortion of the shear tab, twisting of the shear tab, and yield line mechanism of the web supporting member exist simultaneously to produce the overall nonlinear behavior.

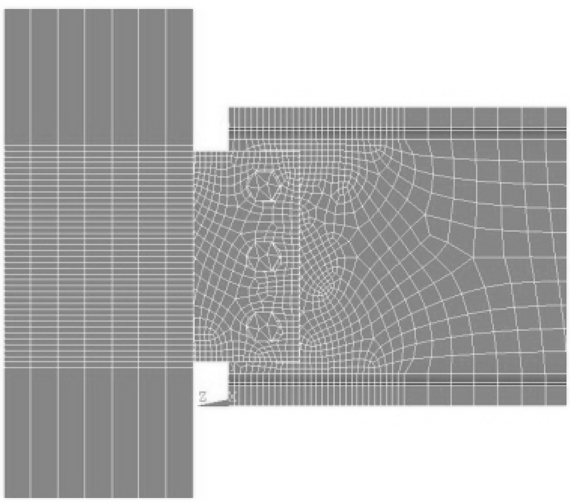

Fig. 8. Connection vicinity for the three-bolt connection.

Figure 9 shows experimental and corresponding finite element results in terms of vertical displacement of the connection plate due to shear. The shear-displacement curve shows that the models and the experiments have the same global yield point in the connection and that they correlate well in the elastic and the plastic ranges. The good correlation is due to the high level of modeling details of the experiments in the finite element model analysis including geometry, boundary conditions, contact surfaces, and applied loads.

It is observed that the FEA results correlate well with the experimental results with an acceptable level of accuracy of 90% and a maximum deviation of 18% for the three-bolt connection and a level of accuracy of 93% for the five-bolt connection.

Shear Load Eccentricity

The shear versus eccentricity graphs are determined from three pairs of strain gauges mounted on the supported beam, as shown in Figures 1 and 2. A linear regression analysis is used to determine the point of zero strain, or zero moment

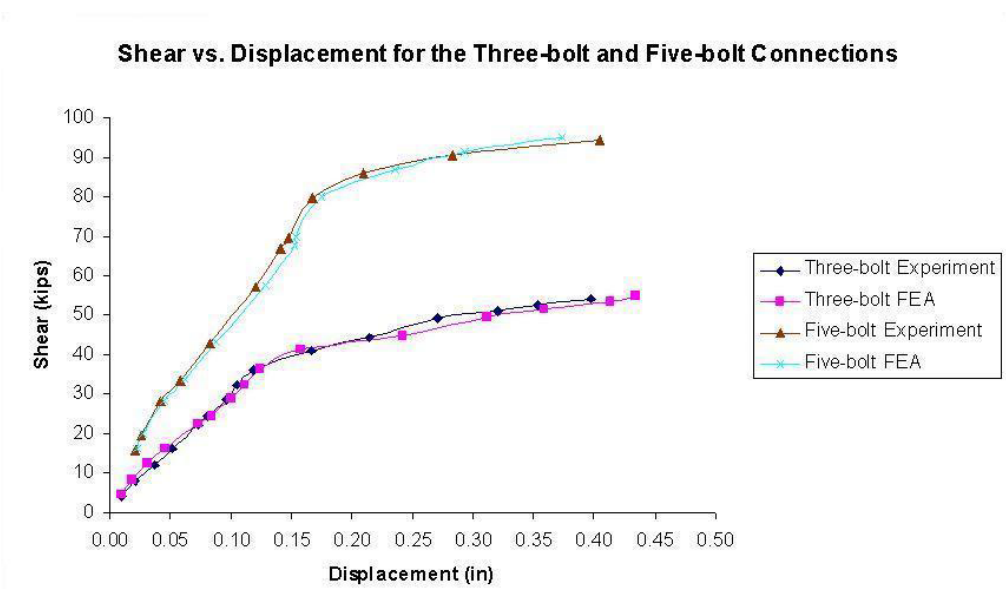

Fig. 9. Shear versus displacement of the connection.

Table 5. Eccentricity Results				
Test	Experiment (in.)	Finite Element (in.)	AISC	
			Rigid-SSL (in.)	Flexible-SSL (in.)
Three-bolt connection	–3.52	–4.18	–4.86	–6.86
Five-bolt connection	–6.02	–5.30	–6.71	–10.04

at each load increment applied to the connection. Equation 1 is used to determine the eccentricity at each load increment using the strain gauge readings.

The eccentricity can be determined at each shear value. The bolt line eccentricity, e_b, is taken as the absolute value of the eccentricity from the shear versus eccentricity graphs. The weld line eccentricity, e_w, is calculated from the distance between the weld center of gravity and the bolt line minus e_b (Sherman and Ghorbanpoor, 2002). The moment experienced by either the bolt group or the weld group can be calculated by multiplying the shear in the connection by the respective eccentricity. It is observed from the shear versus eccentricity curves that there is a shift in the eccentricity values at the early stages; this shift is due to the expected bolt slip that occurs in the connection at the early stages of loading. In most cases, the eccentricity does not change as the shear approaches its ultimate value; this value is very important in evaluating the limit states of the connections.

Another method of determining the location of zero strain, or zero moment, from the FEA is to find the location where the strain value at the top flange of the beam changes sign. The results of these eccentricity values are plotted against eccentricity values obtained from the regression analysis.

The shear eccentricity values do not show good correlation at earlier stages of loading; this is due to the fact that the strain gauges in the experiment do not configure the load at the early stages. At higher load levels the curves converge. The eccentricity values at the ultimate load compare well with the FE findings and the calculated experimental value, as shown in Table 5. This is the critical eccentricity value that is crucial for design considerations. Results at the failure shear force value are within 19% deviation for the three-bolt connection and 17% for the five-bolt connection.

For the zero strain location, direct readings from ANSYS, at the early stages of the loading, show the zero strain at the top of the flange is positive. As the load increases, the top flange will have more compression, and as the connection starts to behave nonlinearly, the location of zero strain, or zero moment, begins to shift. However, the eccentricity results from the location of zero strain readings are slightly different because the linear regression analysis procedure is approximate but within an acceptable range. The experimental and FEA eccentricities of these connections are compared to the AISC eccentricities; as shown in Table 5. It is observed that the behavior of these connections is similar to the behavior of the flexible standard shear tab connections.

Twisting of the Connection Plates

Twisting of the connection plates was significant in the unstiffened connections. This behavior was observed in both experiments and the FEA. In the experiments by Sherman and Ghorbanpoor, shear versus twist curves were plotted to study the twist in the shear tab. The twist behavior was studied by monitoring the readings in the LVDTs mounted at both sides of the top flange of the beam. Ideally, if there is no twist, the LVDT values should be the same; however, in investigating the unstiffened extended shear tab connections, there was always a difference in these values and in some cases the difference was high, especially for the five-bolt connection. This was observed also from the FEA deflection results at similar LVDT locations. The twist in the shear tab is due to the fact that the shear tab and the beam's web are not in the same plane, which results in a twisting action in the shear tab. The twist failure mode was observed in the extended shear tabs and not observed in the standard shear tabs because the distance between the bolt line and the supporting member in the extended shear tabs was large compared to the standard shear tabs.

In the FEA it was easier to study the twist in the shear tab by monitoring the lateral displacement at the top and the bottom of the shear tab. Figures 10 and 11 show the lateral displacement in the shear tab at failure for the three-bolt and five-bolt connection, respectively. The figure shows that the difference in the lateral displacement values is 0.6 in. for the three-bolt connection and 0.64 in. for the five-bolt connection when compared to the experimental output. Figure 12 shows the twist behavior of the shear tab and the supporting girder just before failure.

Nonlinearity

Studying the nonlinear behavior for the extended shear tab connections is challenging in terms of modeling. Nonlinear behavior in the FE models was monitored by studying the shear-displacement curves and by calculating the stresses and plastic deformations at different locations in the connections. Experimentally, connections were loaded to failure and experienced nonlinear behavior. The nonlinear behavior is evident in the shear versus displacement curves as shown in Figure 9.

The importance of nonlinearity appears in identifying the failure modes of each connection. Principal strains were monitored at the location shown in Figure 3. In the experimental work, the first principal strains were obtained from the measured strains using strain gauges 201, 202, and 203 (Sherman and Ghorbanpoor, 2002). In the FE analysis the first principal strains were measured directly at the same location. Figure 13 shows the shear versus principal strains for the three- and the five-bolt connections. The results show that the shear tab has yielded at the location and the figure shows good agreement between the experimental and the FE analysis results. This criterion is used to determine if the shear yield criterion is a failure mode for these connections. The results show that shear yield is a failure mode for both the three- and five-bolt connections.

High stresses and plastic deformation were also observed at bolts in all connections studied, which show that the bolts undergo nonlinear behavior and plasticity. The stresses and deformations in the bolts are shown in Figures 14 and 15. These stresses exceed the yield strength of the bolts and the shear tab. Plasticity was also observed in the shear tabs and

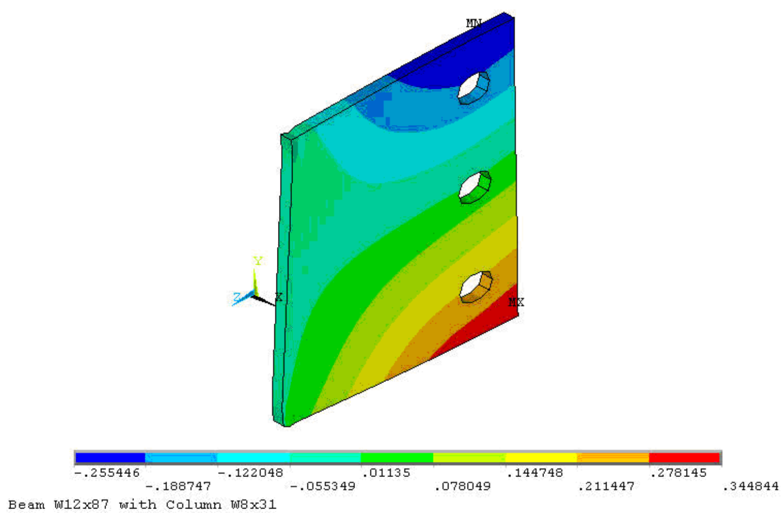

Fig. 10. Deflection of the shear tab for the three-bolt connection twist failure mode.

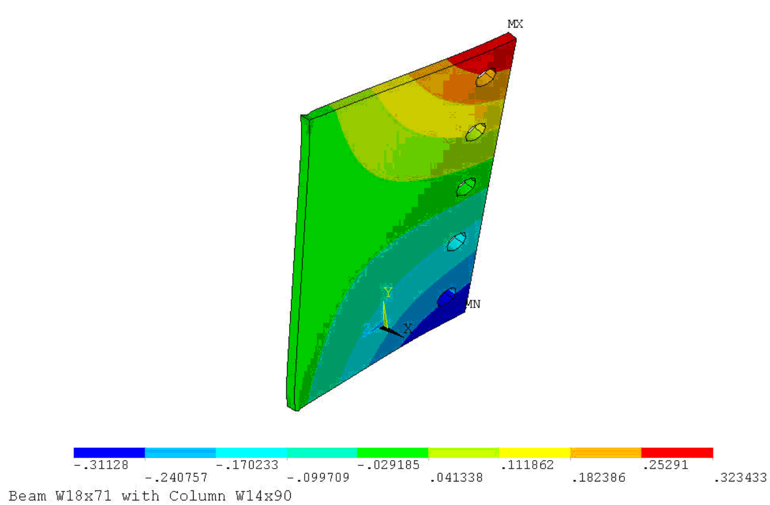

Fig. 11. Deflection of the shear tab for the five-bolt connection twist failure mode.

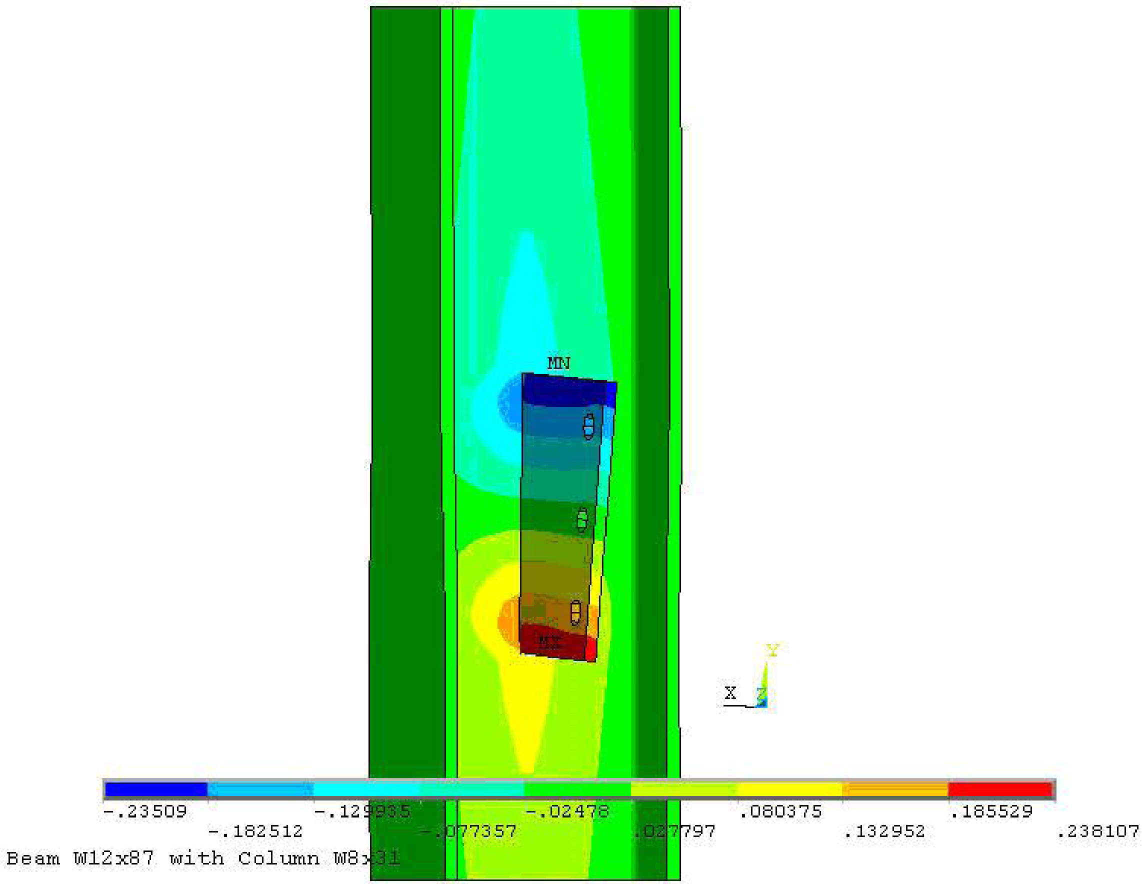

Fig. 12. Twist in the shear tab for the three-bolt connection just before failure.

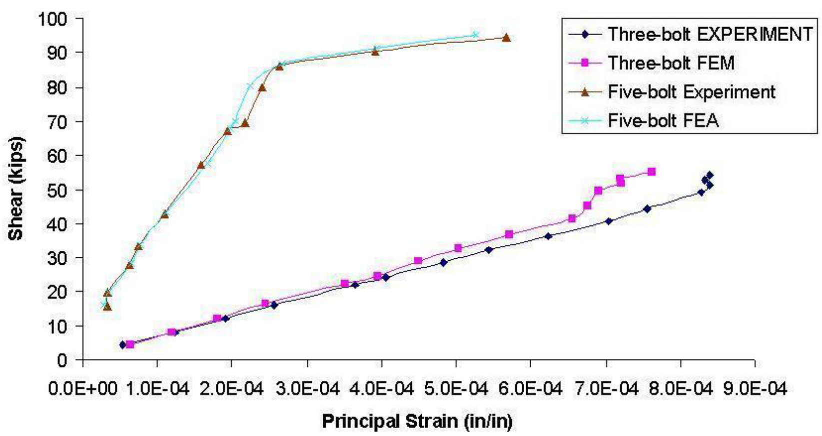

Fig. 13. Shear versus principal strain in the shear tab for the three-bolt and five-bolt connections.

the supporting columns at the top and the bottom tip of the shear tab. This is due to the load transformation from the shear tab to the supporting columns. As a result of this, plastic deformations developed, causing the column web failure mechanism. This behavior was identical in both experiments and FEA, as shown in Figures 16 and 17 (three-bolt connection). Figure 18 shows the stresses in the web of the column for the five-bolt connection. The stresses reach 70 ksi in both tension and compression.

Tables 6 and 7 present the results of strain gauges 107, 108, 109, and 110. The results show the accuracy of the FE model. Due to the high twist and distortion of the shear tab, strain gauge 110 was damaged and dislocated in the experiment; therefore, there is a significant difference between the experimental and FEA results at this location. The strain gauge values indicate twist at the top, bottom, front, and back of the shear tab.

Failure Modes

In experiments, the shear versus displacement, shear versus twist, and shear versus rotation curves were important in determining ultimate shear capacities, point of global yielding and failure modes. The shear value when either the shear-displacement or shear-twist curve approaches a level condition is taken as the ultimate shear capacity. These curves are important in identifying the failure modes. For example, twisting of the shear tab is identified as a primary failure mode if a flattening of the shear-twist curve occurred before the shear-displacement curve. However, if the shear-displacement curve leveled off before the shear-twist curve, shear yield of the shear tab is identified as a failure mode. If the shear-rotation curves indicated high values for rotation in the support member, then a yield line mechanism in the web of the support member will be identified as a primary failure mode. Because most of the experiment failed

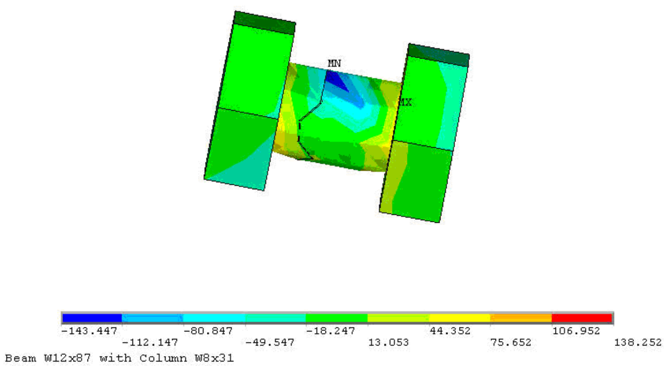

Fig. 14. Bolt shear failure mode in FEA.

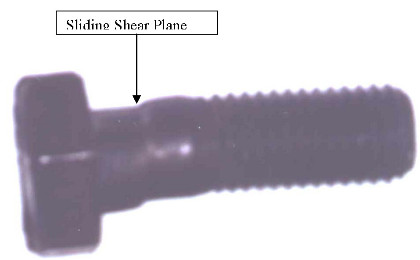

Fig. 15. Bolt shear failure mode in experiment.

Fig. 16. Web mechanism and plasticity in the shear tab for the three-bolt connection in FEA.

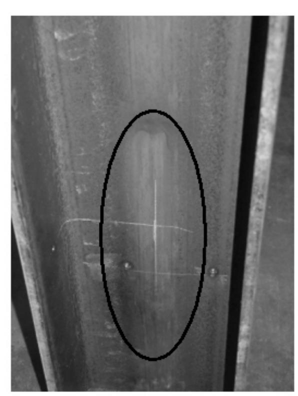

Fig. 17. Web mechanism and plasticity in the shear tab for the three-bolt connection in experiment.

Table 6. Shear Tab Strain Gauge Results for the Three-Bolt Connection									
Strain Gauge		**Point Load (kips)**							
		5.4	**10**	**15**	**20**	**27.3**	**30**	**35.5**	**39.6**
107	**Experimental**	7.00E-05	9.03E-05	2.27E-04	2.30E-04	3.62E-04	3.87E-04	4.47E-04	4.66E-04
	ANSYS	–8.40E-05	1.10E-04	2.10E-04	2.12E-04	3.52E-04	3.70E-04	4.17E-04	4.50E-04
Difference		*–220%*	*22%*	*–7%*	*–8%*	*–3%*	*–4%*	*–7%*	*–3%*
108	**Experimental**	4.52E-05	1.41E-04	1.72E-04	2.99E-04	4.43E-04	4.87E-04	5.84E-04	6.43E-04
	ANSYS	–1.45E-05	–1.90E-04	1.64E-04	2.45E-04	4.28E-04	3.95E-04	5.56E-04	6.35E-04
Difference		*–132%*	*–235%*	*–5%*	*–18%*	*–3%*	*–19%*	*–5%*	*–1%*
109	**Experimental**	–9.20E-05	–1.48E-04	–2.68E-04	–3.61E-04	–5.21E-04	–5.56E-04	–6.35E-04	–6.65E-04
	ANSYS	–7.90E-05	–1.58E-04	–2.48E-04	–3.45E-04	–5.11E-04	–5.50E-04	–6.12E-04	–6.48E-04
Difference		*–14%*	*7%*	*–7%*	*–4%*	*–2%*	*–1%*	*–4%*	*–3%*
110	**Experimental**	–1.15E-06	–8.01E-05	–1.84E-04	–2.93E-04	–4.89E-04	–5.45E-04	–6.66E-04	–7.38E-04
	ANSYS	–1.81E-05	–1.28E-05	–2.76E-04	–2.62E-04	–4.41E-04	–4.12E-04	–5.98E-04	–7.20E-04
Difference		*1474%*	*–84%*	*50%*	*–11%*	*–10%*	*–24%*	*–10%*	*–2%*
Rosette[1]	**Experimental**	5.34E-05	1.24E-04	1.91E-04	2.56E-04	3.64E-04	4.05E-04	4.83E-04	5.44E-04
	ANSYS	6.46E-05	1.20E-04	1.81E-04	2.44E-04	3.51E-04	3.95E-04	4.49E-04	5.04E-04
Difference		*21%*	*–3%*	*–5%*	*–5%*	*–4%*	*–2%*	*–7%*	*–7%*

[1]Rosette principal strain.

Table 6 (Continued). Shear Tab Strain Gauge Results for the Three-Bolt Connection								
Strain Gauge		**Point Load (kips)**						
		44.6	**50.4**	**54.9**	**60.6**	**63.2**	**65**	**67**
107	**Experimental**	4.93E-04	5.16E-04	5.66E-04	6.33E-04	6.97E-04	7.54E-04	8.39E-04
	ANSYS	4.71E-04	5.00E-04	5.76E-04	6.42E-04	7.31E-04	7.45E-04	8.72E-04
Difference		*–4%*	*–3%*	*2%*	*1%*	*5%*	*–1%*	*4%*
108	**Experimental**	7.27E-04	8.67E-04	9.93E-04	1.17E-03	1.31E-03	1.39E-03	1.48E-03
	ANSYS	6.86E-04	7.20E-04	0.001124	1.38E-03	1.22E-03	1.40E-03	1.29E-03
Difference		*–6%*	*–17%*	*13%*	*18%*	*–7%*	*0%*	*–13%*
109	**Experimental**	–6.97E-04	–6.91E-04	–7.55E-04	–8.59E-04	–9.50E-04	–1.06E-03	–1.17E-03
	ANSYS	–6.35E-04	–6.77E-04	–8.02E-04	–8.08E-04	–9.45E-04	–9.49E-04	–1.08E-03
Difference		*–9%*	*–2%*	*6%*	*–6%*	*–1%*	*–10%*	*–8%*
110	**Experimental**	–8.41E-04	–8.88E-04	–8.90E-04	–9.52E-04	–9.88E-04	–1.02E-03	–1.07E-03
	ANSYS	–7.06E-04	–8.66E-04	–8.56E-04	–1.22E-03	–1.10E-03	–1.18E-03	–1.01E-03
Difference		*–16%*	*–2%*	*–4%*	*28%*	*12%*	*16%*	*–6%*
Rosette[1]	**Experimental**	6.23E-04	7.03E-04	7.55E-04	8.28E-04	8.40E-04	8.33E-04	8.40E-04
	ANSYS	5.70E-04	6.55E-04	6.76E-04	6.91E-04	7.21E-04	7.20E-04	7.62E-4
Difference		*–9%*	*–7%*	*–10%*	*–17%*	*–14%*	*–14%*	*–9%*

[1]Rosette principal strain.

Table 7. Shear Tab Strain Gauge Result for the Five-Bolt Connection								
Strain Gauge		Point Load (kips)						
		19.5	24.3	34.5	41.1	52.3	69.7	81.9
107	Experimental	2.76E-04	2.75E-04	4.32E-04	6.19E-04	8.12E-04	1.14E-03	1.34E-04
	FEM	–8.40E-05	2.71E-04	4.86E-04	5.27E-04	6.95E-04	1.18E-03	1.39E-03
Difference		*130%*	*–1%*	*13%*	*–15%*	*–14%*	*4%*	*3%*
108*	Experimental							
	FEM	1.05E-05	1.11E-05	1.96E-05	3.03E-05	6.33E-05	1.55E-04	5.82E-04
Difference								
109	Experimental	–0.000404	–4.04E-04	–5.89E-04	–7.52E-04	–1.01E-03	–1.38E-03	–1.59E-03
	FEM	–4.01E-04	–4.29E-04	–6.32E-04	–7.89E-04	–1.09E-03	–1.41E-03	–1.48E-03
Difference		*5%*	*6%*	*7%*	*5%*	*8%*	*2%*	*–7%*
110	Experimental	0.000187	1.87E-04	2.14E-04	1.79E-04	1.52E-04	7.74E-05	4.05E-05
	FEM	2.03E-04	2.28E-04	2.56E-04	2.14E-04	1.78E-04	9.10E-05	5.26E-05
Difference		*17%*	*22%*	*20%*	*20%*	*17%*	*18%*	*30%*
Rosette[1]	Experimental	3.43E-05	3.45E-05	6.25E-05	7.41E-05	1.09E-04	1.58E-04	1.94E-04
	FEM	2.80E-05	3.61E-05	6.51E-05	7.75E-05	1.12E-04	1.67E-04	1.97E-04
Difference		*18%*	*5%*	*4%*	*5%*	*3%*	*6%*	*2%*

[1]Rosette principal strain.
*Bad guage in experiment.

Table 7. (Continued). Shear Tab Strain Gauge Result for the Five-Bolt Connection						
Strain Gauge		Point Load (kips)				
		85	97	105	110.3	115.1
107	Experimental	1.44E-03	1.59E-03	1.78E-03	1.11E-03	9.08E-04
	FEM	1.44E-03	1.42E-03	1.65E-03	1.23E-03	1.03E-03
Difference		*0%*	*–11%*	*–7%*	*11%*	*13%*
108*	Experimental					
	FEM	6.90E-04	9.70E-04	1.33E-03	1.53E-03	2.15E-03
Difference						
109	Experimental	–1.61E-03	–1.80E-03	–1.95E-03	–1.67E-03	–1.74E-03
	FEM	–1.48E-03	–2.21E-03	–2.03E-03	–1.55E-03	–1.61E-03
Difference		*–8%*	*23%*	*4%*	*–7%*	*–7%*
110	Experimental	–1.77E-05	3.48E-05	–2.23E-05	–3.80E-04	–3.89E-04
	FEM	–2.04E-04	–5.16E-04	–9.77E-04	–1.57E-03	–1.96E-03
Difference		*1053%*	*–1583%*	*4281%*	*313%*	*404%*
Rosette[1]	Experimental	2.18E-04	2.39E-04	2.64E-04	3.92E-04	5.67E-04
	FEM	2.05E-04	2.25E-04	2.66E-04	3.94E-04	5.27E-04
Difference		*–6%*	*–6%*	*1%*	*1%*	*–7%*

[1]Rosette principal strain.
*Bad guage in experiment.

in shear yield, and few experiments failed in twist and yield line mechanism of the supporting member's web, the shear-displacement curve is obtained from the FEA to determine the connection capacities. Because the FEA gives full field results at every location, the failure modes are determined visually based on monitoring ultimate stresses and deflections at critical locations of the structural members.

Several failure modes are observed in three-bolt and five-bolt connections. The primary failure modes for the three-bolt connection are bolt shear, web mechanism, and twist of the shear tab. Figure 14 shows the stress distribution in the vertical *y*-direction for the three-bolt connection bolts. The shear and the tensile stress distributions obtained from the FE model, show that the stress in the bolt exceeds the ultimate tensile stress obtained from a tensile test for the bolt, which is 139 ksi. The computed ultimate shear stress value from mechanics theory, for the same bolt's tensile stress, is half the above value. The FE stress value ranges between 112 and 143 ksi; which exceeds the ultimate strength of the bolt both in tension and in shear. Figure 15 shows the deformation of the bolt when it failed in bolt shear in the experiments.

Figures 19 and 20 show yield and plasticity in the shear tab in both FEA and experiments, respectively. The high contour stress regions are the locations of high stresses in the *z*-direction that eventually affect the supporting web. Deterioration occurred in the web of the supporting columns; Figures 16 and 17 show the deterioration in the back of the column's web in both experiments and in the FEA, respectively.

Twist in the shear tab is also observed to be a failure mode for both models, but it was more severe for the five-bolt connection; twist was its primary failure mode. The twist was observed at early stages of loading during the experiments and in the FEA, which was evident in the beam's flanges. Figure 21 shows the twist in the FE model, and Figure 22 shows the twist failure mode in the experiment.

Bolt shear and web mechanism are secondary failure modes for the five-bolt connection in the experiments. However, the FEA indicates that the bolt shear failure mode appears to be the primary failure mode as well as the twist failure mode. The web mechanism is observed to be a secondary failure mode in the FEA.

CONCLUSIONS

This paper presents a 3D, FE, nonlinear model that is capable of predicting the failure mechanism in a 3D simulation of steel connections, bolts, and structural members. This model is unique in addressing the failure of a shear tab in the plastic region, which considers the bolt pretensioning and nonlinear contact analysis. Having verified the results obtained from the FE model with conducted experiments for the same structural connections, the model presents a powerful tool that can handle a variety of steel connections commonly used in steel construction.

In the elastic and plastic ranges, the FE model is well constructed and seems to be adequate in producing results in good agreement with the experimental results. Confidence in the 3D, nonlinear, FE results is due to the excellent level

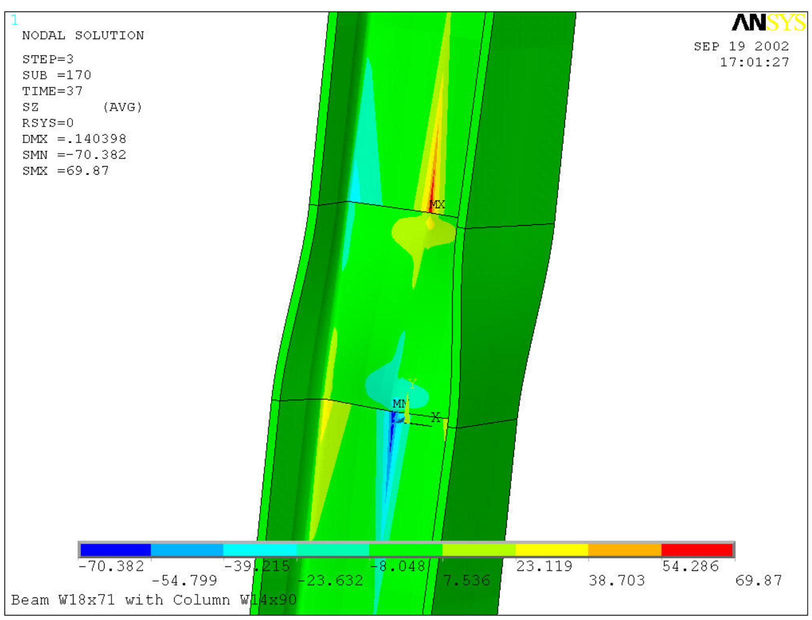

Fig. 18. Web mechanism and plasticity in the shear tab for the five-bolt connection in FEA.

of detailing done to accurately reproduce the geometry of all the structural components as prescribed by the experimental setup and the AISC specifications, and the accurate description of the stress-strain diagram of all steel grades used. The attention given to the level and location of mesh refinement is adequate and contributed to the good agreement between FE and experimental results in the plastic region. Special attention is given to the description of the boundary conditions, loads, coefficient of friction between surfaces, and pretensioning modeling.

The results obtained from the FEA for the load-deflection curves of the beam are within 10% deviation of the experi-

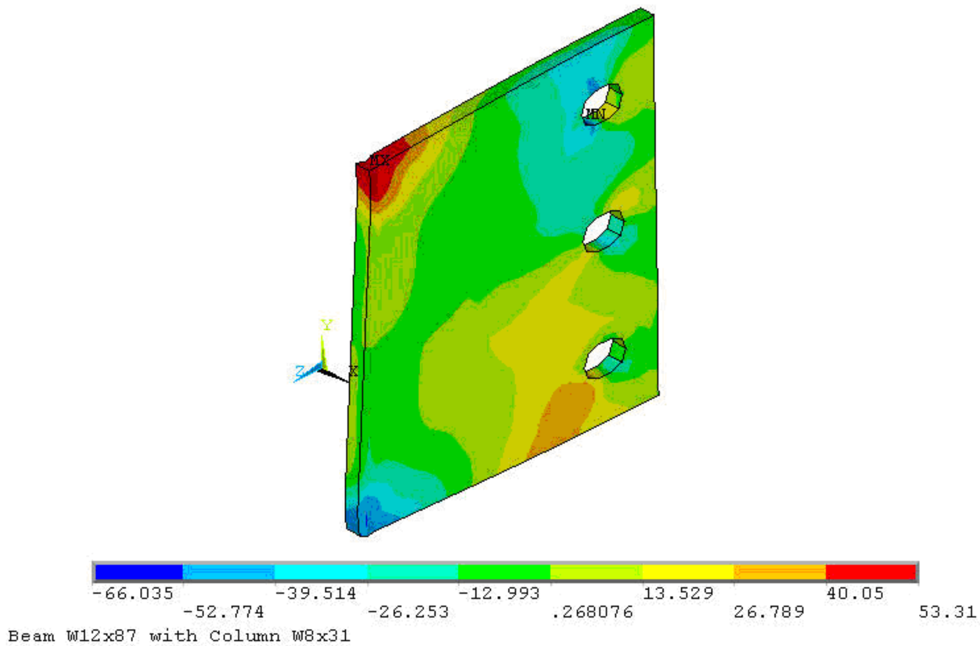

Fig. 19. Plasticity in the shear tab for the three-bolt connection in FEA.

Fig. 20. Plasticity in the shear tab for the three-bolt connection in experiment.

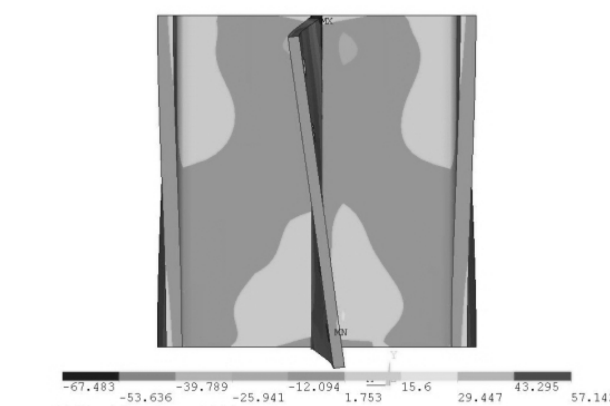

Fig. 21. Twist failure mode in shear tab for the five-bolt connection in FEA.

mental results for the 3U model with a maximum deviation of 18%, and within 8% deviation for the 4U model. An even stronger correlation is observed when comparing the results for principal strains. These results are within 7% deviation for both models. The computation of eccentricity by the FE model shows better agreement at high load levels with a percentile deviation of 19% for both models. The finite element model is capable of predicting the failure modes of the structures, as the models failed in similar failure modes as in the experiments. The comparison between the computational analysis and the experiments is better than expected. Sources of errors can be related to both FEA and the experimental setup.

This paper has identified the relevant parameters needed in a 3D, FE model that makes the analyses of such steel connections of different material types and configurations possible, without the need to rely heavily on expensive experimental investigation. The model is extended to study the behavior of stiffened deep connections that may include a variety of bolt configurations under different cases of loading.

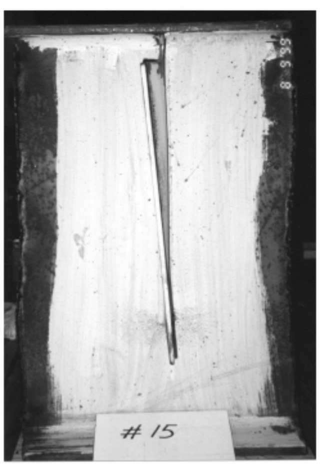

Fig. 22. Twist failure mode in shear tab for the five-bolt connection in experiment.

REFERENCES

AISC (1994), *Manual of Steel Construction, Load and Resistance Factor Design*, Vol. I and Vol. II, Second Edition, AISC, Chicago, IL.

Sherman, D. and Ghorbanpoor, A. (2002), "Design of Extended Shear Tabs," *Research Report RR3095*, American Institute of Steel Construction, Inc., Chicago, IL.

Dally, J.W. (1978), *Experimental Stress Analysis*, 2nd Edition, McGraw-Hill Book Company.

ANSYS (2000), *User Manual,* Version 5.7, ANSYS Corporation, Pittsburgh, PA.

ANSYS (2000), *Theory Manual*, Version 5.7, ANSYS Corporation, Pittsburgh, PA.

ANSYS (2001), *Training Manual*, ANSYS Corporation, Pittsburgh, PA.